JACS
JOURNAL OF THE AMERICAN CHEMICAL SOCIETY
Article
pubs.acs.org/JACS

Intracellular Fate of Spherical Nucleic Acid Nanoparticle Conjugates

Xiaochen A. Wu,[‡] Chung Hang J. Choi,[†,‡] Chuan Zhang, Liangliang Hao, and Chad A. Mirkin*

International Institute for Nanotechnology and Department of Chemistry, Northwestern University, 2145 Sheridan Road, Evanston, Illinois 60208, United States

Supporting Information

ABSTRACT: Spherical nucleic acid (SNA) nanoparticle conjugates are a class of bionanomaterials that are extremely potent in many biomedical applications. Their unique ability to enter multiple mammalian cell types as single-entity agents arises from their novel three-dimensional architecture, which consists of a dense shell of highly oriented oligonucleotides chemically attached typically to a gold nanoparticle core. This architecture allows SNAs to engage certain cell surface receptors to facilitate entry. Here, we report studies aimed at determining the intracellular fate of SNAs and the trafficking events that occur inside C166 mouse endothelial cells after cellular entry. We show that SNAs traffic through the endocytic pathway into late endosomes and reside there for up to 24 h after incubation. Disassembly of oligonucleotides from the nanoparticle core is observed 16 h after cellular entry, most likely due to degradation by enzymes such as DNase II localized in late endosomes. Our observations point to these events being likely independent of core composition and treatment conditions, and they do not seem to be particularly dependent upon oligonucleotide sequence. Significantly and surprisingly, the SNAs do not enter the lysosomes under the conditions studied. To independently track the fate of the particle core and the fluorophore-labeled oligonucleotides that comprise its shell, we synthesized a novel class of quantum dot SNAs to determine that as the SNA structures are broken down over the 24 h time course of the experiment, the oligonucleotide fragments are recycled out of the cell while the nanoparticle core is not. This mechanistic insight points to the importance of designing and synthesizing next-generation SNAs that can bypass the degradation bottleneck imposed by their residency in late endosomes, and it also suggests that such structures might be extremely useful for endosomal signaling pathways by engaging receptors that are localized within the endosome.

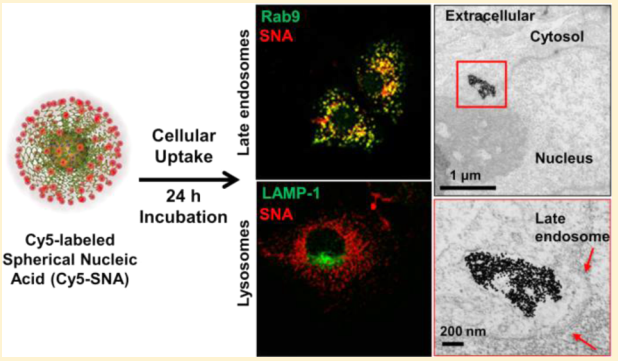

INTRODUCTION

Spherical nucleic acid (SNA) conjugates represent an emerging class of bionanomaterials that typically consist of two types of fundamental building blocks, oligonucleotides and inorganic nanoparticle cores.[1] Due to their ability to naturally enter multiple mammalian cell types without the aid of lipid or cationic transfection agents, SNAs are extremely potent and useful in a variety of biomedical applications. SNAs have been shown to be effective for intracellular diagnostic assays and as novel gene regulation agents.[2−4] We previously postulated a mechanism for endocytosis of SNAs, which involves the specific recognition of their dense oligonucleotide shell by Class A scavenger receptors on the cell membrane as well as their subsequent uptake via the lipid-raft/caveolae pathway.[5] Unfortunately, very little is known about the intracellular events of SNAs following cell entry.

Previous work by others on different classes of nanoparticles has suggested that particle size,[6] shape,[7] density,[8] and surface chemistry[9] can impact cellular entry. However, investigations of the intracellular events that happen to nanoparticles subsequent to their cellular entry are scarce and do not seem to reach a universal consensus. Indeed, it is likely that there is no universal description of biotrafficking for nanoparticles and that all variables must be considered. For example, polymeric nanoparticles can access multiple intracellular compartments, such as the Golgi apparatus, cytosol, and endoplasmic reticulum.[10] Chitosan nanoparticles modified with hydrophobic moieties end up in lysosomes.[11] Protein-coated gold nanoparticles (AuNPs) often get trapped inside endosomes but can be directed elsewhere in the cell through the addition of cell-penetrating peptides or a liposome exterior,[12,13] or even recycled out of the cell.[14] Similarly, lipid nanoparticles containing siRNA have been shown to be largely limited to the endocytic pathway, resulting in recycling.[15] Due to their three-dimensional (3D) oligonucleotide shells, SNAs represent a fundamentally different class of nanomaterial with the ability to engage receptors that other classes of particles often do not. Therefore, SNAs may exhibit a unique profile of intracellular fate, a topic worthy of exploration.

In this work, we synthesized a new class of SNA consisting of a quantum dot (QD) core and a fluorescent oligonucleotide shell (FL-QD-SNA) to support our investigation of the intracellular events that occur following the cellular uptake of

Received: March 25, 2014
Published: May 19, 2014

   dx.doi.org/10.1021/ja503010a | J. Am. Chem. Soc. 2014, 136, 7726−7733

our classic gold SNA (Au-SNA) construct. Specifically, we studied the intracellular trafficking of SNAs in C166 mouse endothelial cells, the signals which dictate trafficking routes, the rate and origins of SNA degradation, and the recycling potential of the material. Based upon the results of these studies, we propose a mechanism by which SNAs are recognized, processed, and distributed within the cell.

RESULTS AND DISCUSSION

SNAs Primarily Traverse to and Accumulate in Late Endosomes upon Cellular Entry. We first studied the intracellular locations of SNAs as a function of incubation time by using C166 cells (mouse endothelial) as a model cell line, under conditions where cells were continuously incubated (no change in medium) with SNAs (10 nM). For this purpose, we prepared Cyanine 5 (Cy5)-labeled SNAs (Cy5-SNAs) made from 5′ Cy5-labeled, single-stranded DNA oligonucleotides (Cy5-ssDNAs) covalently attached to the surface of 13 nm AuNPs (80 ± 5 oligonucleotides per particle). In addition to the Cy5 moiety, these oligonucleotides bear a nontargeting sequence that is antisense to the mRNA transcript of the green fluorescent protein (GFP) (sequence information listed in Table S1). We chose the GFP sequence for our studies because it is irrelevant and non-targeting for the C166 cell-line, which does not contain the gene. Subsequent discussion of SNAs will refer to this sequence unless otherwise specified. By examining whether the fluorescent signals of Cy5-SNAs colocalized with the immunofluorescence of specific protein markers for intracellular compartments with strong literature precedent for nanoparticle accumulation, we were able to delineate the route of trafficking of SNAs inside cells. These protein markers include early endosome antigen 1 (EEA1), Ras-related protein 9 (Rab9), lysosomal-associated membrane protein 1 (LAMP1), and giantin. Their corresponding intracellular compartments are early endosome,[16] late endosome,[17] lysosome,[18] and the trans-Golgi network,[19] respectively.

Our previous work has shown that SNAs are primarily localized in early endosomes after 1−2 h of incubation with cells.[5] In these experiments, the SNAs carry a Cy5 dye (red), and the cells are stained with a complementary dye-labeled (green) marker of interest (in Figure 1A, the marker of interest is EEA1, a protein that localizes exclusively in early endosomes). Here, we demonstrate that SNAs show moderate colocalization with early endosomes from the fourth to 24th hour of incubation (Figure 1A). This continual association with early endosomes suggests that uptake and trafficking are continuous processes. Importantly, strong colocalization of SNAs with Rab9 (protein localizes in late endosomes) was observed after the fourth hour of incubation, and colocalization persisted 24 h post-incubation. Experimentally, we observe a typical cell doubling time of 18 h for C166 cells, and we believe that SNAs largely reside within late endosomes after their departure from early endosomes (Figure 1B, note the orange-yellow color, indicating colocalization of SNAs and Rab-9 marker). Significantly, we did not observe appreciable colocalization between the fluorescent signals of SNAs and markers for lysosomes (LAMP-1) or trans-Golgi network (giantin) over the entire incubation period of 24 h (Figure 1C,D). From these data, we conclude that the probability of SNAs trafficking from early endosomes to the lysosome or trans-Golgi network is low. It is also interesting to note that our data suggest that SNAs do not fully progress through the typical route of the endolysosomal pathway for the degradation of

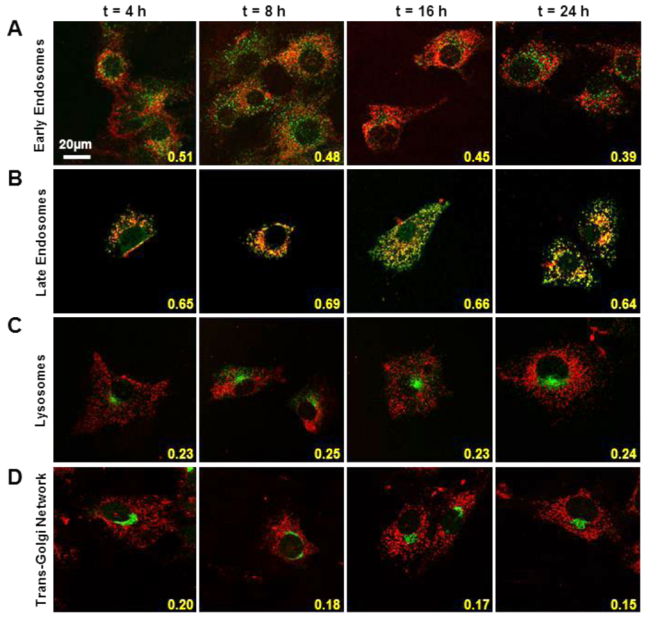

Figure 1. Confocal microscopy of Cy5-labeled Au-SNAs (red) and immunofluorescence staining of organelle markers (green). Markers are EEA1 (early endosome), Rab9 (late endosome), LAMP1 (lysosomes), and giantin (trans-Golgi network.) Most SNAs colocalize with late endosomes during continuous incubation in C166 cells. Some SNA colocalization with early endosomes is observed. SNAs do not colocalize at any time with lysosomes or the trans-Golgi network. Mander's colocalization coefficients are displayed in yellow (>0.6 indicates substantial colocalization.)[34]

biological entities. Instead, over this time period, SNAs stall inside of late endosomes and do not traffic extensively beyond this point.

Transmission electron microscopy (TEM) images for cells collected after continuous treatments of Au-SNAs further reinforce the confocal imaging data. At most time points, the overwhelming majority of SNAs is observed inside perinuclear vesicles measuring from 400 nm to 1 μm in diameter (Figure 2A,C), a size range consistent with the reported average dimension of late endosomes (700 nm).[20] Only a tiny portion of these particles escape the endosomes and are found in the cytosol (Figure S1). Moreover, high-magnification TEM images reveal a key defining ultrastructural feature of late endosomes, the presence of numerous luminal vesicles that resemble multivesicular bodies (MVBs) encapsulated by the late endosomes (Figure 2B). These luminal vesicles mostly measure 50−100 nm across (Figure 2C), fitting literature reports for luminal vesicles characteristic of late endosomes.[21] Structures such as cisternae and electron dense lumens were not seen in association with SNAs, indicating no intracellular trafficking to the trans-Golgi network and mature lysosome, respectively. Moreover, TEM micrographs reveal nanoparticle clusters of increasing sizes as well as decreasing interparticle distances inside late endosomes as a function of incubation time. After 4 h of incubation, SNAs in clusters of 20−30 particles are localized in late endosomes without apparent contact with each other. By contrast, SNAs typically manifest as clusters of ∼300−500 particles accumulated inside late endosomes after 16 h of incubation. In short, upon cellular entry, Au-SNAs that exist in early endosomes as individual particles gradually traverse to late endosomes as clusters of particles in close proximity to one another.

dx.doi.org/10.1021/ja503010a | J. Am. Chem. Soc. 2014, 136, 7726−7733

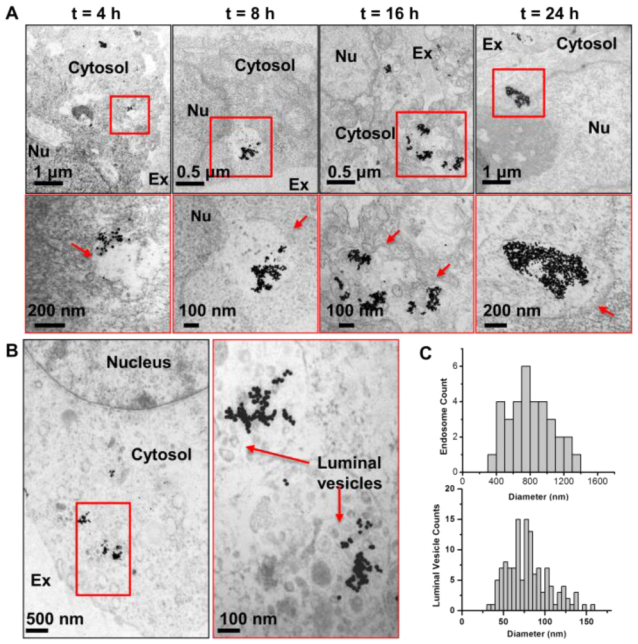

Figure 2. TEM micrographs show intracellular Au-SNAs collect inside increasingly larger and more perinuclear compartments over time. Nu = nucleus, Ex = extracellular space. (A) Most Au-SNAs traffic through increasingly larger, membrane-bound vesicles and remain inside these compartments over 24 h of continuous incubation in C166 cells. Arrows indicate clear membrane boundaries. The bottom panel contains magnified images of the boxed area of the top panel. (B) High magnification of large vesicles inside cells after 16 h incubation. Numerous luminal vesicles and compartment size ranges suggest these are late endosomes. The right panel shows the magnified image of the boxed area of the left panel. (C) Size distribution of (top) endosomes containing Au-SNAs and (bottom) luminal vesicles in these endosomes after long incubations (16–24 h). Sizes of these features align with literature values for late endosomes.

Intracellular Location Likely Does Not Depend Significantly on the Chemical Composition of the Nanoparticle Core or Oligonucleotide Sequence. Following identification of intracellular compartments which house our conventional Au-SNAs after their cellular entry, we set out to preliminarily determine whether trafficking to as well as accumulation in late endosomes without further departure was a phenomenon generalizable to other SNAs with different nanoparticle cores. To do so, we treated cells with two structural variants of the Au-SNA, namely a hollow SNA and an SNA with a CdSe/ZnS QD core (Scheme 1). Hollow SNAs are 3D oligonucleotide-based nanoconstructs obtained by cross-linking multiple alkyne-terminated Cy5-ssDNAs on the surface of an AuNP core that is subsequently dissolved by KCN.[22] Quantum dot SNAs (QD-SNAs) were first synthesized by our group in 1999[23] by covalently attaching oligonucleotides directly to the QD core. Subsequent to that work, we reported a method for non-covalently immobilizing ssDNA on the surface of aliphatic-ligand protected CdSe/ZnS quantum dots by reacting them with amphiphillic polymers, functionalized with DNA.[20,24] Significantly, we have used QD-SNAs and the hollow SNAs to show that the composition and even absence of the nanoparticle core have no appreciable effect on the intracellular fate of SNAs; both SNA structure variants were found to be within late endosomes after 4 h of incubation (Figure 3A, compare Figure 1B).

Scheme 1. Diagrams of SNA Variant Constructs[a]

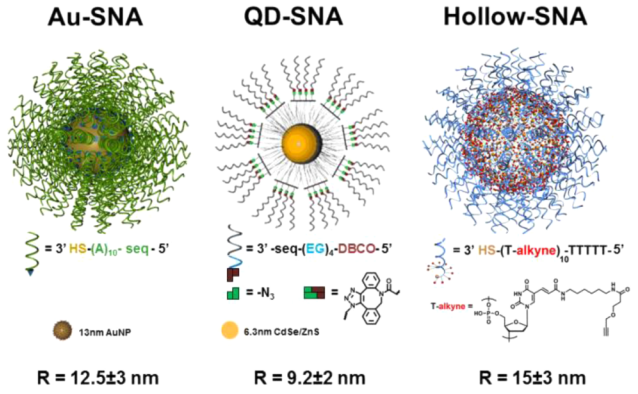

[a]Au-SNA comprises of a 13 nm diameter AuNP core and 3′ thiol terminated ssDNA adsorbed to the surface. QD-SNA comprises of a 7 nm diameter CdSe/ZnS 630 emission QD coated with a layer of azide bearing amphiphilic polymer, which surrounds the surface of aliphatic-ligand protected CdSe/ZnS QD by hydrophobic interactions. ssDNA containing DBCO groups on the 5′ end are attached to the amphiphilic polymer shell by copper-free click chemistry. Hollow SNAs are composed of a T-alkyne crosslinked cage on the 3′ end of ssDNA. Hydrodynamic radii (R) of each construct were measured using dynamic light scattering.

Next, we studied two SNAs composed of different oligonucleotide sequences to determine if there was sequence-specific sorting within the cell. For these experiments, we functionalized AuNP cores with two distinct ssDNA sequences, namely a repeated thymidine sequence (T_{30}) and a sequence antisense to the transcript of the survivin oncogene. T_{30} is not gene targeting, and the survivin sequence exists but is not overexpressed in this cell line. Therefore, these two types of SNAs allow one to probe if sequence makes a significant difference with regard to intracellular SNA fate. Confocal immunofluorescence studies show that these SNAs behave analogously to our GFP sequence SNAs, also trafficking into late endosomes after 4 h of continuous incubation (Figure 3B). TEM micrographs also show the presence of T_{30} SNAs inside of large membrane-bound vesicles (Figure S2). Therefore, the sheer 3D architecture of the oligonucleotides, rather than the sequence information encoded by them, is likely the primary attribute which governs the intracellular trafficking behavior of SNAs. Further in-depth studies are needed to confirm these preliminary findings.

Uptake and Trafficking Are Independent Processes. Next, we considered other mechanisms which could drive endocytic sorting. Previous work has shown that SNA cellular entry is a continuous process.[5] We hypothesized that SNA trafficking into the late endosome could potentially be driven by subsequent waves of SNA uptake. To investigate the effect of continuous uptake on the trafficking of SNAs, we utilized a pulse-chase setup to follow a small window of uptake events. Cells were treated with Au-SNAs (10 nM) for 1 h only and then placed into clean, fresh SNA-free media for different durations of time. Immunofluorescence analysis shows colocalization of SNAs with the early endosomes at the end of the 1 h treatment, but strong colocalization with late endosomes 24 h after the initial treatment with SNAs has ended (Figure 3C). TEM images support this conclusion as Au-SNAs are in small, featureless vesicles as isolated entities at the end of 1 h treatment but collect inside of larger, multivesicular

dx.doi.org/10.1021/ja503010a | J. Am. Chem. Soc. 2014, 136, 7726–7733

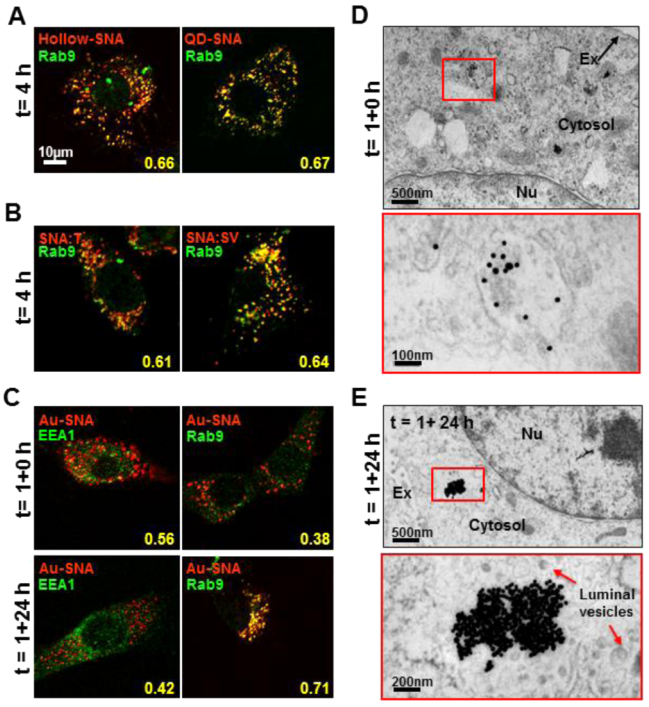

Figure 3. Location analysis for SNA variant constructs and treatment variant in C166 cells. Immunofluorescence Rab9 staining (green) of cells treated with different SNA constructs (red) for 4 h shows that (A) hollow SNAs (no core), QD-SNAs with a CdSe-ZnS core, (B) SNAs consisting of a repeated thymidine sequence (SNA:T_{30}), and SNAs consisting of a sequence antisense to the transcript that encodes the survivin oncogene (SNA:SV) also colocalize strongly with late endosomes. Scale bar = 10 μm for all confocal images. (C) Pulse-chase experiments show Cy5-labeled Au-SNAs that have already entered the cell 1 h postincubation progress in the endocytic cycle. Immunofluorescence staining shows that SNAs colocalize with early endosomes (EEA-1) but not late endosomes (Rab9) after 1 h incubation. They then colocalize with late endosomes but not early endosomes 24 h after the initial incubation of 1 h. Mander's colocalization coefficients are displayed in yellow. (D) Representative TEM micrographs show rare occurrences of Au-SNAs within small compartments as isolated entities after 1 h incubation. (E) Large clusters of Au-SNAs (>200 particles per cluster) are found abundantly in large, perinuclear compartments 24 h after the initial incubation of 1 h. For (D) and (E), the bottom panel contains magnified images of the boxed area of the top panel. Nu = nucleus, Ex = extracellular space.

endosomes after the 24 h treatment-free incubation period (Figure 3D). Treating cells with Au-SNAs for only 4 h also gives similar results (Figure S3). These data show that cells sort SNAs independent of uptake duration or quantity. In other words, C166 cells will naturally sort an overwhelming majority of SNAs from early endosomes to late endosomes unbiased by the stimulus induced by the uptake of subsequent waves of SNAs.

Intracellular Disassembly of SNAs Is Likely Due to Degradation by DNaseII. The late endosome represents an integral part of the cellular degradation pathway and has been shown to eventually fuse with lysosomes.[25] The lumen of the late endosome is known to be an environment that facilitates degradation of biomacromolecules. Acidic pH, presence of catabolic enzymes, and redox active species are just a few characteristic features of the late endosome.[26] Proteins and oligonucleotides have been shown to be extensively degraded due to this environment.[27] We were interested in probing the susceptibility of SNAs to degradation due to their prolonged accumulation inside the late endosomes. From our TEM imaging data in Figure 2, the intracellular aggregation of the AuNP core becomes increasingly prevalent as a function of incubation time, suggesting the possibility of intracellular degradation of the oligonucleotide shell that originally provided steric stabilization to and electrostatic repulsion between SNA nanostructures. To address the issue of degradation, we incubated Cy5-labeled Au-SNAs (also used for the confocal imaging studies in Figure 1) under different chemical conditions and measured how many Cy5-ssDNA strands remain on the surface of the AuNP core after the treatment. Briefly, we centrifuged the chemically treated SNA solution to recover the SNA pellet, dissolved the AuNP core, and quantified the Cy5 fluorescence of the solution against a standard calibration curve. We first subjected Cy5-labeled Au-SNAs to various buffers with pH values ranging from 7.5 to 4.5, a window that covers the essential intracellular compartments expected to be traversed by a SNA along the endolysosomal pathway, including extracellular fluid (pH = 7.4), early endosomes (pH = 5.5−6.0), and late endosomes/lysosomes (pH = 4.5−5.0).[28] After 3 d of incubation, Cy5-SNAs did not show reduction in oligonucleotide loading. We next added Cy5-SNAs to a degassed PBS solution that contains intracellular concentrations of glutathione (1−10 mM)[29] to analyze whether the surplus of thiol groups from glutathione (GSH) in the cell would displace thiolated ssDNA strands off the AuNP surface. For this experiment, the PBS was thoroughly degassed by repeated freeze−thaw cycles to prevent the oxidation of GSH to form dimers (GSSG) in the cell-free environment. Again, after incubation for 1 d, the fluorescence associated with the solution of Cy5-SNAs did not significantly increase, indicating no appreciable oligonucleotide displacement from the particle surface (Figure S4). Thus, change in pH and thiol displacement by glutathione cannot account for the aggregation of Au-SNAs inside the cell.

Finally, we investigated if DNA nucleases natively found in late endosomes or lysosomes may contribute to the degradation of SNAs. Two common nucleases pertinent to DNA degradation are deoxyribonuclease I (DNase I) and deoxyribonuclease II (DNase II). DNase I has been implicated in DNA degradation in the serum, extracellular space, and also in the cytosol of cells.[30] An acidic endonuclease, DNase II is usually found within intracellular compartments, most notably lysosomes.[31] Since late endosomes are able to fuse with other late endosomes or lysosomes,[25] we hypothesize that DNase II is responsible for DNA degradation when SNAs are shuttled to and stalled in the late endosomes. To test this hypothesis, we introduced Cy5-labeled Au-SNAs into a cell-free solution that contains the same concentration of either DNase I or DNase II, each buffered at the appropriate pH required for its proper functioning. After 4 h of incubation, Cy5-labeled Au-SNAs treated with DNase II lost ∼60% of their original oligonucleotide loading, whereas those treated with DNase I lost only ∼25% (Figure 4A). We further showed that, by contrast to the SNA architecture, more than 80% of Cy5-ssDNA of the same nucleotide sequence was degraded after incubation with both enzymes for 4 h. For this assay, free DNA was synthesized with a 3′ molecular quencher of the 5′ dye (see Supporting Information for sequence information) in order to allow for similar percentage degradation calculations as those done with SNAs. Thus, the arrangement of DNA oligonucleotides in the form a dense 3D shell can endow SNAs with

dx.doi.org/10.1021/ja503010a | J. Am. Chem. Soc. 2014, 136, 7726−7733

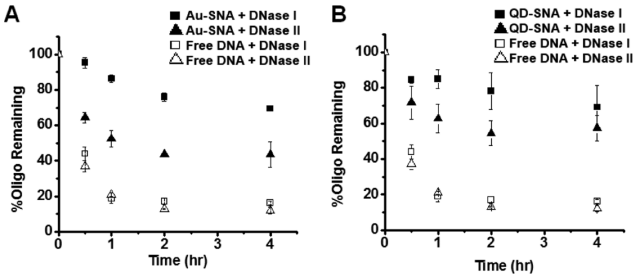

Figure 4. Buffer tests of (A) Au-SNAs and (B) QD-SNAs show that both structure variants on the SNA architecture offer protection against DNase I and II compared to free, single-stranded DNA (ssDNA). DNase degradation profiles for both Au-SNA and QD-SNA are sufficiently similar to suggest that they behave similarly under intracellular enzymatic environments. Note that, in buffer, the SNA architecture is more prone to degradation by DNase II, an enzyme commonly found in late endosomes or lysosomes, than Dnase I, which is usually found in extracellular fluids or the cytosol.

additional stability against enzymatic degradation, but SNAs are less resistant to enzymatic attack by DNase II than DNase I, a conclusion supported by early, less comprehensive work.[32] Note that the time points in these studies may or may not be relevant to the cellular studies since the intracellular concentration of these enzymes has not been reported to date.

We wish to further visualize how intracellular nucleases like DNase II may disassemble the SNA architecture. To achieve this goal, we need to independently track the movement of both the NP core and DNA strands in the cell. While DNA strands can be labeled fluorescently, the innate lack of fluorescence of AuNPs precluded us from visualizing how the DNA strands are falling off the NP core for our classic Au-SNAs by confocal imaging. To circumvent this bottleneck, we synthesized FL-QD-SNAs, a new class of SNA nanostructure that consists of a CdSe/ZnS core (with an emission wavelength of 630 nm) covalently functionalized with fluorescein-labeled ssDNAs. We believe that the FL-QD-SNA serves as a reasonable proxy for the classic Au-SNA due to its similar hydrodynamic diameter (~20 nm) and oligonucleotide loading (70 ssDNA ±4/particle) as previously described.[24] Indeed, DNases exhibit similar activity profiles for both constructs, whereby incubation in DNase II led to more significant reduction in oligonucleotide loading than DNase I (Figure 4A,B). We then treated C166 cells continuously with FL-QD-SNAs and imaged them at various time points. Confocal microscopy shows the FL-QD-SNAs remain largely intact for up to 16 h, as evidenced by overlapping fluorescence signals of the QD core and FL-ssDNAs (Figure 5). After 16 h, the fluorescein signal from the oligonucleotides separates from that of the QD core, with an even larger effect after 24 h. This separation is likely due to DNA cleavage from the SNA by enzymes in the late endosomes, particularly DNase II, which has high activity at low pH. It is important to note that the treatment in this study is continuous, and any newly uptaken QD-SNAs likely influence the true time scale of degradation. In this case, degradation products must build up for a time before they are observable by confocal microscopy.

Differential Recycling of SNA Components. Once we utilized QD-SNAs to establish that the SNA architecture disassemble on the time scale of roughly 16−24 h after entering C166 cells, we returned to Au-SNAs and explored whether their individual components are expelled from the cell. Using the same pulse-chase setup previously described in Figure 3, we

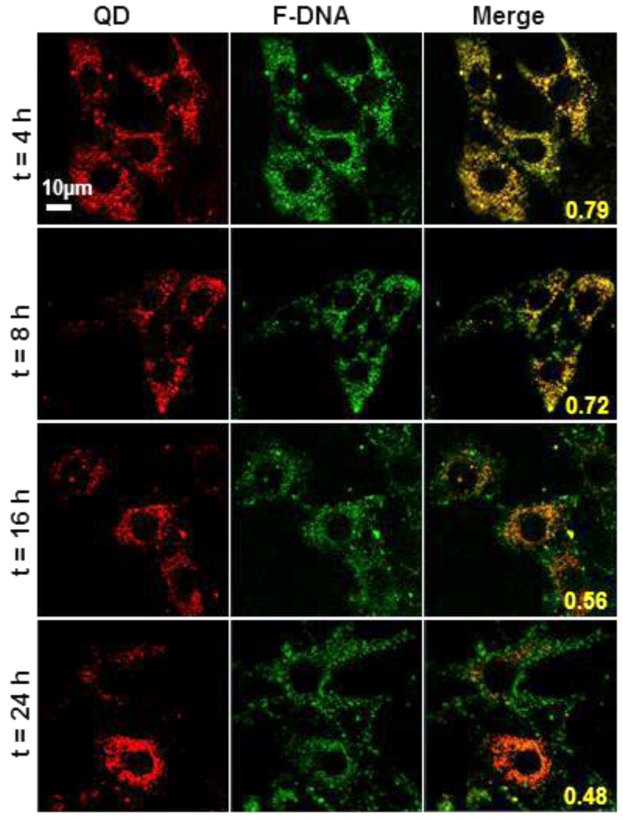

Figure 5. SNAs composed of a CdSe/ZnS QD core and fluorescein-tagged DNA strands (FL-QD-SNAs) are used as a proxy to monitor and visualize the degradation of SNAs in C166 cells. By confocal imaging, the QD core (red) and the fluorescein-tagged oligonucleotides (green) have visibly separated at 16 h and beyond, likely due to enzymatic cleavage. Before 16 h, overlapping signals of QD and FL-DNAs (yellow) indicate that the SNA architecture is largely intact. Mander's coefficients are indicated in yellow for merged images, showing gradual loss of colocalization between the QD and the FL-DNA over time.

tracked the gold content in cells using inductively coupled plasma mass spectrometry (ICP-MS) and quantified the Cy5 fluorescence in cells by spectroscopic analysis. After a 4 h pulse treatment of cells with Cy5-SNAs, we washed out the nanoparticles, grew the treated cells in clean medium, and then divided cell samples for ICP-MS and fluorescence analysis. To exclude the possibility that any observed reduction in the intracellular gold or DNA amount is due to cell division but not actual exocytosis, we treated the cell sample as a population rather than on a single cell basis by ensuring a near-constant density of C166 cells plated for this experiment.

After the 4 h pulse incubation, intracellular gold content remains relatively constant in the cell population over the course of 24 h of growth, indicating no net exocytosis of the AuNP core (Figure 6A). Given our TEM data that reveal increased clustering of AuNP cores, this near-perfect mass balance of intracellular gold content across the entire period of incubation time suggests that the AuNP core of SNAs is continuously sorted from multiple early endosomes of smaller sizes to significantly fewer late endosomes of much larger sizes. The lack of recycling of the AuNP core may stem from the degradation of a large portion of the oligonucleotide shell by intracellular nucleases (most likely, DNase II). Such degradation likely leads to the loss of biological recognition of the SNA

dx.doi.org/10.1021/ja503010a | J. Am. Chem. Soc. 2014, 136, 7726−7733

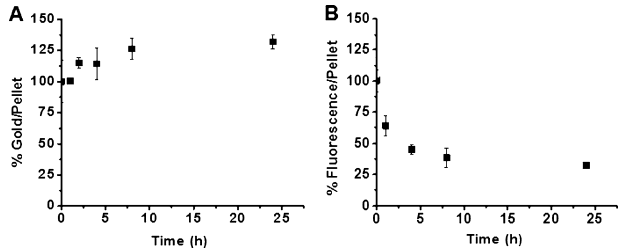

Figure 6. Analysis of material retention inside C166 cells as a function of growth time post-4 h incubation with Cy5-labeled Au-SNAs. (A) Gold content in a single cell population (pellet) remains fairly constant over time. Slight increases may be due to uptake of residual SNAs loosely adhered to the plastic of the tissue culture plate. (B) Fluorescence in a single population of cells sharply decreases after the incubation, indicating the expulsion of Cy5 or DNA fragments into the extracellular space. Error bar indicates the standard deviation from triplicate experiments.

architecture and renders the AuNP core susceptible to colloidal aggregation in the presence of intracellular amounts of salt. Ultimately, these AuNP clusters may not traffic efficiently due to there being no known cellular receptors for this material. By contrast, Cy5 fluorescence is observed to rapidly decrease in the cell lysates if the SNA treatment is discontinued after 4 h (Figure 6B). This decline in fluorescence likely results from degradation products of DNase cleavage that are expelled from the cell either by active transport or diffusion, but not via any recycling pathway based on our confocal imaging data presented in Figure 1. Diffusion seems unlikely as the confocal images presented in Figure 5 reveal punctate spots rather than homogeneous patches of fluorescence, which would be indicative of release into the cytoplasm.

Moreover, we measured the fluorescence of the culture medium collected from the same pulse-chase experiment at different time points after the initial incubation of 4 h. The fluorescence of the medium steadily increases over time after the removal of Cy5-SNAs, thus adding credence to the notion that there is net exocytosis of free Cy5 moieties or processed DNA fragments to the medium (Figure S5).

CONCLUSIONS

From our studies, we have shown that SNAs enter into the endocytic pathway after entry into the cell. SNAs progress largely into late endosomes, which is their final intracellular location over the 24 h time frame considered. A small, unquantifiable portion of these particles escape the endosome and are found in the cytosol. These are the entities that are likely responsible for knockdown in both antisense and RNAi mediated gene regulation pathways. Both immunofluorescence and TEM ultrastructural analysis support this conclusion. Moreover, SNAs traffic along this route and reach the late endosomes, independent of the surface oligonucleotide sequences and the core compositions studied here. Our pulse-chase experiments also show that the intracellular fate of SNAs is guided only by the single-entity agent alone and seems invariant to the quantity of SNAs uptaken. Finally, we show that SNAs are partially broken down by nucleases within the late endosome, and degradation products are differentially processed by the cellular transport machinery: the core is retained in the late endosome, while the dye or oligonucleotide fragments are cleared from the cell, at least for this cell line.

The SNA architecture can function successfully as a gene regulation construct, in part due to the increased stability of the oligonucleotides on SNAs as compared to their free forms. This allows them a longer intracellular residency time. The observation that the vast majority of SNAs are tied up in the endosome suggests that they particularly potent gene regulation agents. Indeed, a small amount escapes the endosome, which accounts for their activity in antisense and likely siRNA pathways. Any increased availability of SNAs to the cytosol will further boost the therapeutic activity of SNAs, and we pose the design and synthesis of SNAs capable of more efficient endosomal escape as a challenge to the community. The work also has several additional implications. It brings to light the importance of realizing next generation SNAs that can take advantage of their location inside late endosomes, which may include introducing functionalities to modulate processes such as immune activation and exosome packaging.[33] It also underscores the importance of designing synthesizing hollow SNAs or structures with biodegradable cores to avoid the unanticipated consequences of the core materials on cellular function.

EXPERIMENTAL SECTION

Synthesis of Oligonucleotides. DNAs were synthesized on an MM48 oligonucleotide synthesizer (BioAutomation) using standard solid-phase synthesis and reagents (Glen Research). All DNAs were purified using a ProStar high-performance liquid chromatography (HPLC) instrument (Varian) with a Microsorb C18 column (Varian). Table S1 contains detailed sequence information on the DNAs.

Preparation of SNA Nanoconjugates. For gold-SNA nanoconjugates, thiolated DNAs were added to 13 nm citrate-capped AuNPs at a concentration of 1 OD of DNA per mL of 10 nM AuNPs supplemented with 0.5% Tween-20. After stirring at RT for 1 h, the solution was aged with gradual additions of NaCl over 6 h to bring the final NaCl concentration to 0.5 M. Functionalized AuNPs were separated from free DNA strands via dialysis against Nanopure water using a 50 kDa Amicon molecular weight cutoff membrane (Millipore). AuNP and DNA concentrations were determined by measuring their extinction at 524 and 260 nm, respectively, on a Cary 5000 UV−vis spectrophotometer (Agilent). Hollow SNAs were prepared based on published methods.[22] Quantum dot SNA nanoconjugates were also prepared as detailed previously using CdSe-ZnS quantum dots (Ocean Nanotech).[24]

Cell Culture and SNA Treatment. All cell experiments described in this work employ C166 cells (mouse endothelial), which were cultured at 37 °C and 5% CO_2 in DMEM supplemented with 10% FBS and 1% streptomycin/penicillin. To measure the extent of cellular association by ICP-MS, cells were first seeded in a 24-well plate at a population of 5×10^4 cells per well 24 h in advance and incubated with 0.3 mL of SNAs (10 nM in DMEM) per well. To visualize the extent of cellular uptake by TEM, cells were seeded in a 6-well plate at a population of 5×10^5 cells per well and then incubated with 1.5 mL of SNAs (10 nM in DMEM) per well. For both ICP-MS and TEM studies, SNAs were removed at different time points, followed by DMEM rinses, trypsinization for counting using a hemacytometer and centrifugation at 8000 rpm for 5 min to form a cell pellet. For pulse-chase experiments, cells were first treated with 10 nM SNA for either 1 or 4 h, washed twice with DMEM, and replenished with fresh DMEM. The cells were then incubated for the designated duration of time before harvesting them for ICP-MS and TEM studies.

ICP-MS. Cell pellets were digested with 0.3 mL of 3% HCl in concentrated HNO_3 at RT overnight. After adding 5 μL of 5 ppm indium (internal standard) and 5 mL of matrix solution (2% HCl and 2% HNO_3), the Au-197 content of the resultant solution was measured by an X Series II ICP-MS (Thermo Fisher) after subtracting the background gold content of untreated cells. Unless otherwise

dx.doi.org/10.1021/ja503010a | J. Am. Chem. Soc. 2014, 136, 7726−7733

mentioned, reported values represent mean ± SE from the average of three independent experiments.

TEM. Cell pellets were fixed by resuspension in 3.7% paraformaldehyde (PFA) in PBS for 15 min. Cells were then pelleted again by centrifugation at 6000 rpm for 5 min and enrobed in molten 2% agarose at 37 °C. Molten agarose cell mixtures were expressed into water at RT to produce "noodle-shaped" gels for ease of processing. Following this, the cell-containing noodle gels were fixed in 2.5% glutaraldehyde in 100 mM sodium cacodylate buffer (pH = 7.4), stained by 1% OsO_4 and by 0.9% OsO_4 and 0.3% $K_4Fe(CN)_6$, with all steps carried out at 4 °C for 2 h. After gradual dehydration with ethanol and propylene oxide, the cell-containing noodle gels were embedded in Epon 812 resins (Electron Microscopy Sciences) and further polymerized. We deposited 80 nm-thick sections on 200-mesh copper grids (Electron Microscopy Sciences) and stained with 2% uranyl acetate (SPI Supplies) and Reynolds lead citrate for visualization under a JEM 1230 microscope (JEOL) using a beam voltage of 80 kV. An Orius SC 1000 CCD camera (Gatan) was used to record the images. Endosome and luminal vesicle diameter measurements were taken using ImageJ and freehand blob identification. Diameter is defined as the average of *x*- and *y*-direction feret diameter. Data were binned into bins ∼5% of average measurement.

Confocal Microscopy and Immunofluorescence. Seeded in a 35 mm FluoroDish (World Precision Instruments), cells were incubated with 10 nM of Cy5-SNAs or Cy5-Hollow-SNA in complete DMEM for different time points. Cells were rinsed with PBS, fixed in 3.7% PFA in PBS for 15 min, and imaged under a Zeiss LSM 510 inverted confocal scanning microscope. The excitation wavelength of Cy5-SNAs was 633 nm, and the corresponding emission filter was 660−710 nm. To track the colocalization of SNAs with intracellular proteins, after incubation with 10 nM Cy5-SNAs for different durations of time, cells were rinsed with PBS, fixed in 3.7% PFA in PBS, and permeated with 0.1% Triton X-100 for 10 min. After blocking with 2% BSA in PBS for 1 h, cells were stained with a primary antibody against the protein marker of interest at 5 μg/mL (1% BSA in PBS) overnight at 4 °C. If necessary, after rinses with 0.05% Tween-20 in PBS, cells were stained with an AlexaFluor 488-labeled secondary antibody (Invitrogen Alexa Fluor 488 Goat Anti-Rabbit IgG (H+L)) at 1 μg/mL (1% BSA in PBS) for 1 h at RT. The excitation wavelength of the secondary antibody was 488 nm, and the corresponding emission filter was 500−550 nm. The primary antibodies include rabbit against EEA1 (Abcam ab2900), rabbit against Rab9 (Santa Cruz Biotechnology FL-201), rabbit against LAMP1 (Abcam ab24170), and rabbit against Giantin (Abcam ab24586). To measure the extent of colocalization between the fluorescence signals of SNAs and protein markers, the Zen Digital Imaging (Zeiss) software allows for the calculation of the Manders overlap coefficient.[34] An overlap coefficient higher than 0.6 indicates strong colocalization.[35] To probe the intracellular fate of the individual components of QD-SNAs (i.e., the QD) core and the fluorescein-labeled oligonucleotides), cells were incubated with 10 nM QD-SNAs in DMEM for different durations of time. Following the same rinsing, fixation, and permeation procedures as listed above, the cells were imaged under a confocal scanning microscope. The excitation wavelengths for QD and fluorescein are 633 and 488 nm, respectively. The corresponding emission filters for QD and fluorescein are 660−710 nm and 500−550 nm, respectively.

Oligonucleotide Quantification. 10−12 nmoles of Cy5-labeled SNAs were treated with DNase I (New England Biolabs M0303S) or DNase II (Sigma D4138) (5U/rxn) for set time points. 1% SDS was added to denature the enzymes and stop degradation. All SNAs were pelleted at 10 000 × *g* and washed with water. Pellets were resuspended in a cleaving buffer (100 mM KCN and 100 mM DTT) to dissolve the gold core. After solution had cleared, the Cy5 fluorescence of the oligonucleotides was read on a Synergy H4Multimode Microplate Reader (Bio-TEK) to determine the quantity of oligo lost due to DNase activity. Free oligos were assayed in a similar manner in which a quencher (Dabycl) was conjugated to the opposite (3′) end of the oligo to suppress fluorescence. Oligo cleavage was calculated through increase of fluorescence as quencher and fluorophore are separated. For QD-SNA, 0.5% HCl was used to dissolve the QD core and dismantle the SNA. Following acid treatment, pH was normalized to neutral using NaOH before reading for fluorescein fluorescence.

■ ASSOCIATED CONTENT

Ⓢ Supporting Information

Synthesized DNA sequences in this work, additional TEM images, cell-free SNA stability assays, and recycling of fluorescent SNA oligonucleotide fragments. This material is available free of charge via the Internet at http://pubs.acs.org.

■ AUTHOR INFORMATION

Corresponding Author

chadnano@northwestern.edu

Present Address

[†]Department of Electronic Engineering (Biomedical Engineering), The Chinese University of Hong Kong, Shatin, New Territories, Hong Kong, China.

Author Contributions

[‡]These authors contributed equally.

Notes

The authors declare no competing financial interest.

■ ACKNOWLEDGMENTS

C.A.M. acknowledges support from the Center for Cancer Nanotechnology Excellence (CCNE) initiative of National Institutes of Health (NIH) Awards U54 CA119341 and U54 CA151880, Dixon Translational Research Grants Initiative, the Nanoscale Science and Engineering Centers (NSEC) initiative of National Science Foundation Award EEC-0647560, the Prostate Cancer Foundation, NIAMS/NIH Grants R01AR060810 and R21AR062898, and Defense Advanced Research Planning Agency Awards N66001-11-1-4189 and HR0011-13-2-0018, the International Institute for Nanotechnology at Northwestern University, and the Nonequilibrium Energy Research Center (NERC), an Energy Frontier Research Center funded by the U.S. Department of Energy, Office of Science, Office of Basic Energy Sciences Award DE-SC0000989. C.H.J.C. acknowledges a postdoctoral research fellowship from The Croucher Foundation. L.H. is a Howard Hughes Medical Institute International Student Research Fellow and acknowledges a Ryan Fellowship from Northwestern University. We thank Charlene Wilke of Biological Imaging Facility (BIF) for assistance in ultramicrotomy. ICP-MS measurements and confocal imaging were performed at the Quantitative Bioelemental Imaging Center (Northwestern University). TEM imaging was performed at the BIF (Northwestern University).

■ REFERENCES

(1) Cutler, J. I.; Auyeung, E.; Mirkin, C. A. *J. Am. Chem. Soc.* **2012**, *134*, 1376.

(2) Rosi, N. L.; Giljohann, D. A.; Thaxton, C. S.; Lytton-Jean, A. K. R.; Han, M. S.; Mirkin, C. A. *Science* **2006**, *312*, 1027.

(3) Prigodich, A. E.; Seferos, D. S.; Massich, M. D.; Giljohann, D. A.; Lane, B. C.; Mirkin, C. A. *ACS Nano* **2009**, *3*, 2147.

(4) Zheng, D.; Giljohann, D. A.; Chen, D. L.; Massich, M. D.; Wang, X.-Q.; Iordanov, H.; Mirkin, C. A.; Paller, A. S. *Proc. Natl. Acad. Sci. U.S.A.* **2012**, *109*, 11975.

(5) Choi, C. H. J.; Hao, L.; Narayan, S. P.; Auyeung, E.; Mirkin, C. A. *Proc. Natl. Acad. Sci. U.S.A.* **2013**, *110*, 7625.

(6) Chithrani, B. D.; Ghazani, A. A.; Chan, W. C. W. *Nano Lett.* **2006**, *6*, 662.

(7) Champion, J. A.; Mitragotri, S. *Proc. Natl. Acad. Sci. U.S.A.* **2006**, *103*, 4930.
(8) Choi, C. H. J.; Alabi, C. A.; Webster, P.; Davis, M. E. *Proc. Natl. Acad. Sci. U.S.A.* **2010**, *107*, 1235.
(9) Xiao, K.; Li, Y.; Luo, J.; Lee, J. S.; Xiao, W.; Gonik, A. M.; Agarwal, R. G.; Lam, K. S. *Biomaterials* **2011**, *32*, 3435.
(10) Cartiera, M. S.; Johnson, K. M.; Rajendran, V.; Caplan, M. J.; Saltzman, W. M. *Biomaterials* **2009**, *30*, 2790.
(11) Nam, H. Y.; Kwon, S. M.; Chung, H.; Lee, S.-Y.; Kwon, S.-H.; Jeon, H.; Kim, Y.; Park, J. H.; Kim, J.; Her, S.; Oh, Y.-K.; Kwon, I. C.; Kim, K.; Jeong, S. Y. *J. Controlled Release* **2009**, *135*, 259.
(12) Nativo, P.; Prior, I. A.; Brust, M. *ACS Nano* **2008**, *2*, 1639.
(13) Krpetić, Ž.; Saleemi, S.; Prior, I. A.; Sée, V.; Qureshi, R.; Brust, M. *ACS Nano* **2011**, *5*, 5195.
(14) Bartczak, D.; Nitti, S.; Millar, T. M.; Kanaras, A. G. *Nanoscale* **2012**, *4*, 4470.
(15) Sahay, G.; Querbes, W.; Alabi, C.; Eltoukhy, A.; Sarkar, S.; Zurenko, C.; Karagiannis, E.; Love, K.; Chen, D.; Zoncu, R.; Buganim, Y.; Schroeder, A.; Langer, R.; Anderson, D. G. *Nat. Biotechnol.* **2013**, *31*, 653.
(16) Mu, F.-T.; Callaghan, J. M.; Steele-Mortimer, O.; Stenmark, H.; Parton, R. G.; Campbell, P. L.; McCluskey, J.; Yeo, J.-P.; Tock, E. P. C.; Toh, B.-H. *J. Biol. Chem.* **1995**, *270*, 13503.
(17) Barbero, P.; Bittova, L.; Pfeffer, S. R. *J. Cell Biol.* **2002**, *156*, 511.
(18) Carlsson, S. R.; Fukuda, M. *J. Biol. Chem.* **1989**, *264*, 20526.
(19) Linstedt, A. D.; Mehta, A.; Suhan, J.; Reggio, H.; Hauri, H.-P. *Mol. Biol. Cell* **1997**, *8*, 1073.
(20) Ganley, I. G.; Carroll, K.; Bittova, L.; Pfeffer, S. *Mol. Biol. Cell* **2004**, *15*, 5420.
(21) Russell, M. R. G.; Nickerson, D. P.; Odorizzi, G. *Curr. Opin. Cell Biol.* **2006**, *18*, 422.
(22) Cutler, J. I.; Zhang, K.; Zheng, D.; Auyeung, E.; Prigodich, A. E.; Mirkin, C. A. *J. Am. Chem. Soc.* **2011**, *133*, 9254.
(23) Mitchell, G. P.; Mirkin, C. A.; Letsinger, R. L. *J. Am. Chem. Soc.* **1999**, *121*, 8122.
(24) Zhang, C.; Macfarlane, R. J.; Young, K. L.; Choi, C. H. J.; Hao, L.; Auyeung, E.; Liu, G.; Zhou, X.; Mirkin, C. A. *Nat. Mater.* **2013**, *12*, 741.
(25) Luzio, J. P.; Rous, B. A.; Bright, N. A.; Pryor, P. R.; Mullock, B. M.; Piper, R. C. *J. Cell Sci.* **2000**, *113*, 1515.
(26) Runquist, E. A.; Havel, R. J. *J. Biol. Chem.* **1991**, *266*, 22557.
(27) Tjelle, T. E.; Brech, A.; Juvet, L. K.; Griffiths, G.; Berg, T. *J. Cell Sci.* **1996**, *109*, 2905.
(28) Mellman, I.; Fuchs, R.; Helenius, A. *Annu. Rev. Biochem.* **1986**, *55*, 663.
(29) Hwang, C.; Sinskey, A. J.; Lodish, H. F. *Science* **1992**, *257*, 1496.
(30) Takeshita, H.; Yasuda, T.; Nakajima, T.; Hosomi, O.; Nakashima, Y.; Kishi, K. *Biochem. Mol. Biol. Int.* **1997**, *42*, 65.
(31) Evans, C. J.; Aguilera, R. J. *Gene* **2003**, *322*, 1.
(32) Seferos, D. S.; Prigodich, A. E.; Giljohann, D. A.; Patel, P. C.; Mirkin, C. A. *Nano Lett.* **2008**, *9*, 308.
(33) Alhasan, A. H.; Patel, P. C.; Choi, C. H. J.; Mirkin, C. A. *Small* **2014**, *10*, 186.
(34) Manders, E. M. M.; Verbeek, F. J.; Aten, J. A. *J. Microsc.* **1993**, *169*, 375.
(35) Zinchuk, V.; Zinchuk, O. In *Current Protocols in Cell Biology*; John Wiley & Sons, Inc.: Hoboken, NJ, 2001; Vol. *39*, p 4.19.1.